LETTER
SPACE PHYSICS

Earth and Planetary Physics
2: 469–478, 2018
doi: 10.26464/epp2018045

The Electric Field Detector (EFD) onboard the ZH-1 satellite and first observational results

JianPing Huang[1,2*], JunGang Lei[3*], ShiXun Li[3], ZhiMa Zeren[4], Cheng Li[3], XingHong Zhu[5], and WeiHao Yu[1,6]

[1]Institute of Crustal Dynamics, China Earthquake Administration, Beijing 100085, China;

[2]Key Laboratory of Crustal Dynamics, China Earthquake Administration, Beijing 100085, China;

[3]Lanzhou Institute of Physics, China Academy of Space Technology, Gansu 730000, China;

[4]Institute of Earthquake Forecasting, China Earthquake Administration, Beijing 100036, China;

[5]DFH Satellite Co., Ltd., Beijing 100094, China;

[6]Institute of Disaster Prevention, Hebei 101601, China

Abstract: Previous studies have reported that, before or after occurrences of strong earthquakes, some low earth orbit satellites recorded ionospheric disturbances, including electromagnetic emissions and plasma fluctuations over the epicenter region or its conjugate point. Theoretically speaking, due to some electromagnetic coupling effect, electromagnetic emissions from the earthquake preparation zone could propagate from the lithosphere to the atmosphere, and could reach the ionosphere, even up to the inner magnetosphere. This paper introduces the electric field detector (EFD) onboard the ZhangHeng-1 satellite (ZH-1). The EFD is designed to measure electric field fluctuations within the broad frequency range of DC to 3.5 MHz, divided into 4 channels: ULF (DC–16 Hz), ELF (6 Hz–2.2 kHz), VLF (1.8 kHz–20 kHz) and HF (18 kHz–3.5 MHz). The sampling rates of the channels are 125 Hz, 5 kHz, 50 kHz and 10 MHz, respectively. The EFD includes 4 spherical probes mounted on a over 4.5 m boom and an electronic box inside the satellite module. The resolution of the EFD is 1 $\mu V{\cdot}m^{-1}{\cdot}Hz^{-1/2}$ at frequencies from DC to 16 Hz, and the sensitivity is 0.1 $\mu V{\cdot}m^{-1}{\cdot}Hz^{-1/2}$ at frequencies from 6 Hz to 2.2 kHz, 0.05 $\mu V{\cdot}m^{-1}{\cdot}Hz^{-1/2}$ in the band 1.8 kHz to 20 kHz, and 0.1$\mu V{\cdot}m^{-1}{\cdot}Hz^{-1/2}$ from 20 kHz to 3.5 MHz. The dynamic range from DC to 20 kHz is over 120 dB, and over 96 dB from 20 kHz to 3.5 MHz. The EFD has two observation modes: survey mode and burst mode. The survey mode concentrates primarily on electric field power density values; the burst mode provides high sampling rate waveform data. The detailed configuration of the EFD onboard the ZH-1 is also introduced in this paper. During the six months' orbit test phase, the EFD recorded a number of natural electromagnetic emissions. Preliminary analysis of these data suggests that the EFD performs well onboard the ZH-1 and is meeting the requirements of the scientific objectives of ZH-1.

Keywords: EFD; payload; ZhangHeng-1; sensitivity

Citation: Huang, J. P., Lei, J. G., Li, S. X., Zeren, Z. M., Li, C., Zhu, X. H., and Yu, W. H. (2018). The Electric Field Detector (EFD) onboard the ZH-1 satellite and first observational results. *Earth Planet. Phys.*, *2*(6), 469–478. http://doi.org/10.26464/epp2018045

1. Introduction

In recent decades, a number of studies have suggested that natural electromagnetic emissions induced by Earth's seismic activity can be detected not only by ground-based receivers but can also be captured by satellites that fly over event epicenters. Previous studies report electromagnetic signals related to strong earthquakes over a very broad frequency range, from DC/Ultra Low Frequency (ULF) (Fraser-Smith et al., 1990; Ouyang XY and Shen XH, 2015; Surkov et al., 2003; Zhang X et al., 2011, 2014), to Extreme Low Frequency (ELF) and Very Low Frequency (VLF) (Molchanov et al., 1993; Parrot, 1995; Zeren ZM et al., 2012), and even to Low Frequency (LF) and High Frequency (HF) (Maekawa et al., 2006; Biagi et al., 2001; Takano et al., 2002), or even Very High Frequency (VHF) (Yamada et al., 2002).

The DEMETER satellite, launched by France in 2004, also carries an electric field experiment (ICE), to measure the electric field at frequency bands from DC/ULF (0–15 Hz), ELF (15 Hz–1 kHz), VLF (15 Hz–17.4 Hz) to HF (10 kHz–3.175 MHz) (Berthelier et al., 2005). The DEMETER ICE observations show that an electric field detector can capture field fluctuations during earthquakes, lightning activities, geomagnetic storms and other space events (Bhattacharya et al., 2007; Hayakawa et al., 2010; Kasahara et al., 2008; Sarkar and Gwal, 2010; Rozhnoi et al., 2010; Zhang X et al., 2012; Zeren ZM et al., 2014, 2017).

With scientific objectives similar to those of DEMETER, the China Seismo-Electromagnetic Satellite (CSES) was launched on February 2nd, 2018. The CSES is also called ZH-1, named after an ancient Chinese seismologist, ZhangHeng (in Chinese), about 2000 years ago. The ZH-1 is the first Chinese space-based platform devoted to monitoring ionospheric disturbances induced by seismic activities or other natural sources. Eight payloads aboard the ZH-1

Correspondence to: J. P. Huang, xhhjp@126.com
J. G. Lei, lei7412@163.com
Received 05 OCT 2018; Accepted 05 NOV 2018.
Accepted article online 28 NOV 2018.

measure the electromagnetic field as well as plasma and energetic particles in the ionosphere. The EFD, one of main ZH-1 payloads, same as the search coil magnetometer and magnetic flux gate (Shen XH et al., 2018). The variety of scientific payloads aboard the ZH-1 provides a great opportunity to the scientific community to observe the geophysical field from the lithosphere to the upper ionosphere, to detect pre-seismic low frequency electromagnetic signals, and to study possible seismic ionospheric disturbance mechanisms.

The specific scientific objective of the EFD is to measure electric field disturbances over a broad frequency band (DC/ULF/EFL/VLF/HF) with high sampling rates. The EFD has two observation modes: survey and burst. The survey mode concentrates primarily on electric field power spectrum density (PSD) values; the burst mode provides high sampling rate waveform data. Specifically, at ULF, ELF and HF, in both survey and burst modes the EFD detects the same type of electric field scientific data at the same sampling rates. At the ULF and ELF frequency bands, the raw scientific data include the voltage of each of four electric balls. At the HF band, it provides only a set of PSD values with a time resolution of 2.048 s. At the VLF frequency band, the survey mode provides only the PSD value; the burst mode provides only waveform data.

The resolution of the EFD is 1 $\mu V{\cdot}m^{-1}{\cdot}Hz^{-1/2}$ at frequencies from DC to 16 Hz, and the sensitivity is 0.1 $\mu V{\cdot}m^{-1}{\cdot}Hz^{-1/2}$ at frequencies from 6 Hz to 2.2 kHz, 0.05 $\mu V{\cdot}m^{-1}{\cdot}Hz^{-1/2}$ in the band 1.8 kHz to 20 kHz, and 0.1 $\mu V{\cdot}m^{-1}{\cdot}Hz^{-1/2}$ from 20 kHz to 3.5 MHz. The dynamic range from DC to 20 kHz is over 120 dB, and over 96 dB from 20 kHz to 3.5 MHz. Section 2 presents a detailed description of the EFD.

2. Description of the EFD

2.1 EFD Sensor Structure

The EFD onboard ZH-1 was developed by the Lanzhou Institute of Physics and is designed to measures the spatial low frequency electric field in the frequency range from DC to 3.5 MHz. The EFD consists of 4 spherical sensors, with embedded pre-amplifier electronics, and associated electronics to fulfill the onboard signal-processing requirements.

The 4 spherical sensor probes are each mounted on the end of a 4.5-meter stacer boom, in order to deploy the electric probes sufficiently far away from the spacecraft plasma sheath to avoid interference from the satellite platform, including its solar panel. This configuration of electric field probes has been used in many satellite or rocket experiments, for example DEMETER's electric field detector ICE (Berthelier et al., 2005).

Each probe is a spherical aluminum electrode, with a diameter of 60 mm, as shown in Figure 1. The cylinder (the blue one in Figure 1) is 20 mm in diameter and 71mm in length. The spherical probe is coated with DAG 213 (a material that minimizes the surface work function difference).

Each sphere is mounted at the end of its 4.5 m boom through a cylindrical stub, which is used as the interface between the sensor and the boom.

2.2 Working Principle of the EFD

The EFD works on the active double-probe principle, in which the electric field is measured by the voltage difference between two probes a known distance from each other. The working principle of the EFD is given in Figure 2.

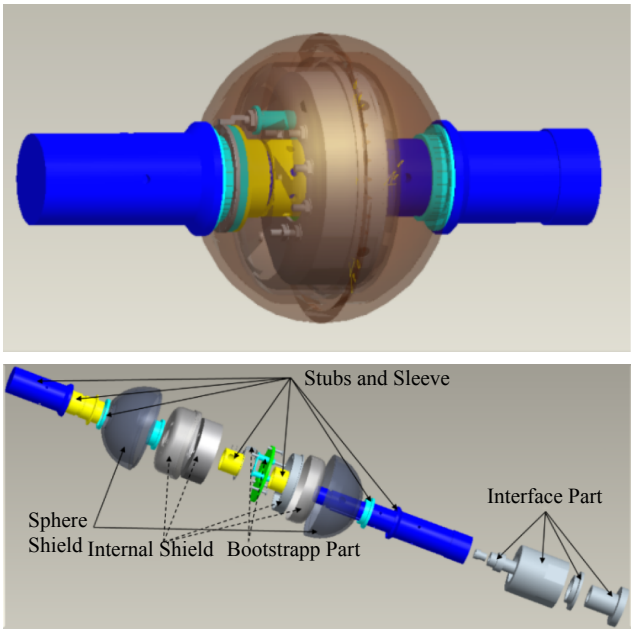

Figure 1. The structure of the EFD's spherical sensor probe. Top: the outer appearance of the EFD probe, Bottom: the internal structure of the EFD probe.

From Figure 2, the plasma voltage of the two probes V_{p1} and V_{p2} are given by formulae (1) and (2):

$$V_{p1} = V_S + V_{x1} - V_1, \tag{1}$$

$$V_{p2} = V_S + V_{x2} - V_2. \tag{2}$$

Combining formulae (1) and (2), we get

$$V_{p1} - V_{p2} = (V_{x1} - V_{x2}) - (V_1 - V_2). \tag{3}$$

We define E as the natural electric field detected by the EFD payload; d is the distance between the two probes. E is then computed by the formula:

$$E = \frac{(V_{p1} - V_{p2})}{d}. \tag{4}$$

By combining formulae (3) and (4), E is given by the formula:

$$E = \frac{(V_{x1} - V_{x2}) - (V_1 - V_2)}{d}. \tag{5}$$

We assume that the surface voltages of the two probes, relative to the satellite platform, are nearly the same:

$$V_1 \approx V_2. \tag{6}$$

So E can be written as:

$$E = \frac{(V_{x1} - V_{x2})}{d}. \tag{7}$$

It must to be pointed out that E includes the voltage induced by the satellite's motion in the magnetic field, which means that there exist a $v{\times}B$ effect, so we have to remove it:

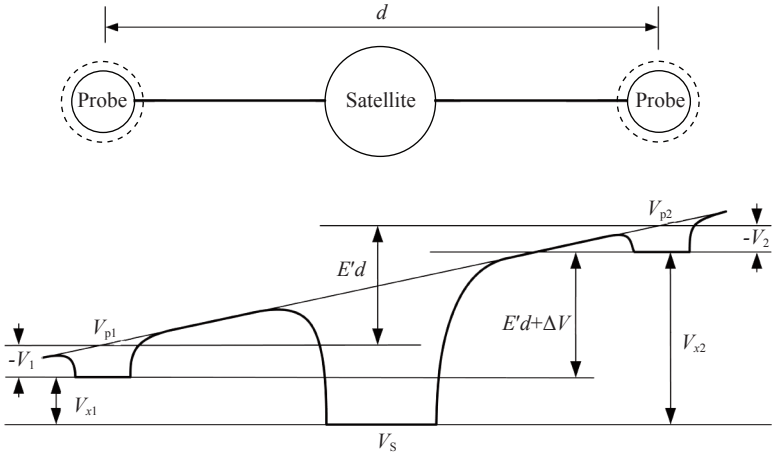

Figure 2. Scheme for double-probes detection principle. V_{p1} and V_{p2}: plasma voltages near the two probes; V_1 and V_2: probe surface voltages relative to plasma, V_S: satellite's ground voltage; V_{x1} and V_{x2}: surface voltages of probes relative to satellite.

$$E' = E - v \times B, \tag{8}$$

where E' is the real natural electric field we aim to measure, v is the satellite's velocity relative to the Earth, and $\boldsymbol{B}$ is the vector geomagnetic field.

Finally, the spatial electric field:

$$E' = \frac{(V_{x1} - V_{x2})}{d} - v \times B. \tag{9}$$

2.3 Onboard Configuration

Figure 3 shows the detailed EFD configuration onboard the ZH-1 satellite. *X*, *Y*, and *Z* in the satellite coordinate system are defined as: *X* is the flight direction of the satellite, *Z* is the direction from the satellite platform to the Earth, and *Y* is the direction of *Z* crossed with *Y*.

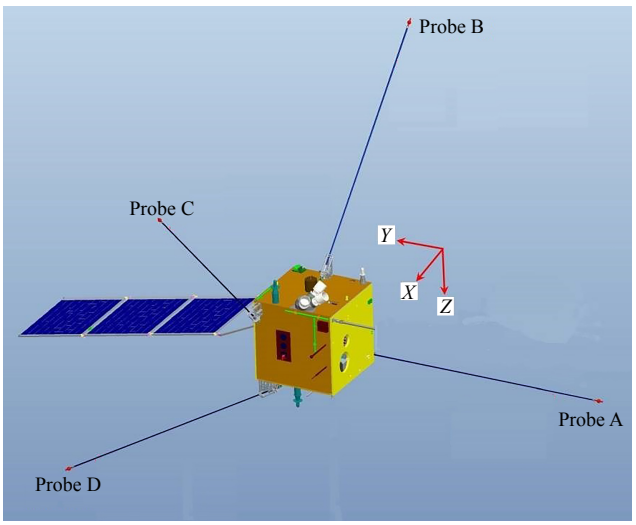

Figure 3. Onboard configuration of EFD. The coordinates in this figure reflect the satellite orbit system.

Table 1 provides the exact location and direction of each probe onboard the ZH-1 satellite. It can been seen from Figure 3 and Table 1 that Probe A is deployed in the *X* plane, and directs to the opposite direction of the *Y* axis; Probe B is located in the *Z* plane at the bottom of satellite platform, with a direction of 45° between the -*X* and -*Z* axes; Probes C and D are located in the *X* and *Z* planes, respectively. Details are listed in Table 1.

The direction distance between the 4 probes is given in Table 2. The distances between Probes A and B, C, D are 7.315 m, 8.329 m, and 9.566 m, respectively.

Table 1. Boom direction (relative to satellite coordinate)

Probe	Location	Direction
A	In -*X* plane, close to -*Y*+*Z*	Directed to -*Y* axis
B	In -*Z* plane, close to satellite bottom	Directed 45° to both -*X* and -*Z* axis
C	In +*X* plane, close to -*Z*+*Y*	Directed 45° to both -*Z* and +*X* axis
D	In +*Z* plane, close to +*Y*+*X*	Directed 30° with +*Y* axis and 60° with +*Z* axis

Table 2. Distance between probes

Distance	*b*	*c*	*d*
A	7315 mm	8329 mm	9566 mm
B	–	7647 mm	9298 mm
C	–	–	9394 mm

When measuring the potential difference between two of those sensors, the EFD operates as a double probe instrument, as described in Section 2.2: the component of the electric field is determined along the axis defined by the two sensors. The nominal configuration of these 3 components in the EFD's sensor coordinates is the following:

Channel 1: $V_{ab} = V_a - V_b$,

Channel 2: $V_{cd} = V_c - V_d$,

Channel 3: $V_{ad} = V_a - V_d$.

Where *V* is the voltage of the natural electric field, *a*, *b*, *c*, and *d*

represent the probes. The electric field from three directions or channels of sensors is transferred from the probes' voltage values by the coefficient matrix listed below:

$$\boldsymbol{A}=\begin{pmatrix} x_a-x_b & y_a-y_b & z_a-z_b \\ x_c-x_d & y_c-y_d & z_c-z_d \\ x_a-x_d & y_a-y_d & z_a-z_d \end{pmatrix}, \boldsymbol{V}_{\rm SS}=\begin{pmatrix} V_{\rm CH1} \\ V_{\rm CH2} \\ V_{\rm CH3} \end{pmatrix}, \boldsymbol{E}_{\rm SB}=\begin{pmatrix} E_x \\ E_y \\ E_z \end{pmatrix}$$

in which $\boldsymbol{V}_{\rm SS}=\boldsymbol{A}\cdot\boldsymbol{E}_{\rm SB}$ and the coordinates of each probe *a*, *b*, *c*, and *d* in the satellite coordinate system are $\begin{pmatrix} x_a & y_a & z_a \end{pmatrix}$, $\begin{pmatrix} x_b & y_b & z_b \end{pmatrix}$, $\begin{pmatrix} x_c & y_c & z_c \end{pmatrix}$, $\begin{pmatrix} x_d & y_d & z_d \end{pmatrix}$.

From the EFD's sensor coordinates to satellite coordinates, the transfer matrix is:

$$\boldsymbol{A}^{-1}=\begin{pmatrix} 1.375 & -1.434 & 1.328 \\ -0.027 & 0.019 & 0.102 \\ -0.672 & 0.876 & -0.721 \end{pmatrix}.$$

2.4 Onboard Data Processing Unit

The electronics of the EFD, including the DPU (Data Processing Unit), encompass an analog part with a set of filters and amplifiers to process the analog signals from the sensors, and a digital part to carry out the waveform, power spectra computation, and telemetry interfaces. The block diagram of DPU's analog part is shown in Figure 4.

According to the different data sampling rates at ULF, ELF, VLF and HF, as well as the data package solutions onboard the ZH-1, the work time of the EFD is classified into 3 layers, as shown in Figure 5.

The working period (WP) normally lasts 247.808 s. It is equally divided into 121 sub-working periods, each one 2.048 s. The first of the 121 sub-working periods is called the bias-current corrected period (BCP). During this BCP, the bias current will be set at a con-

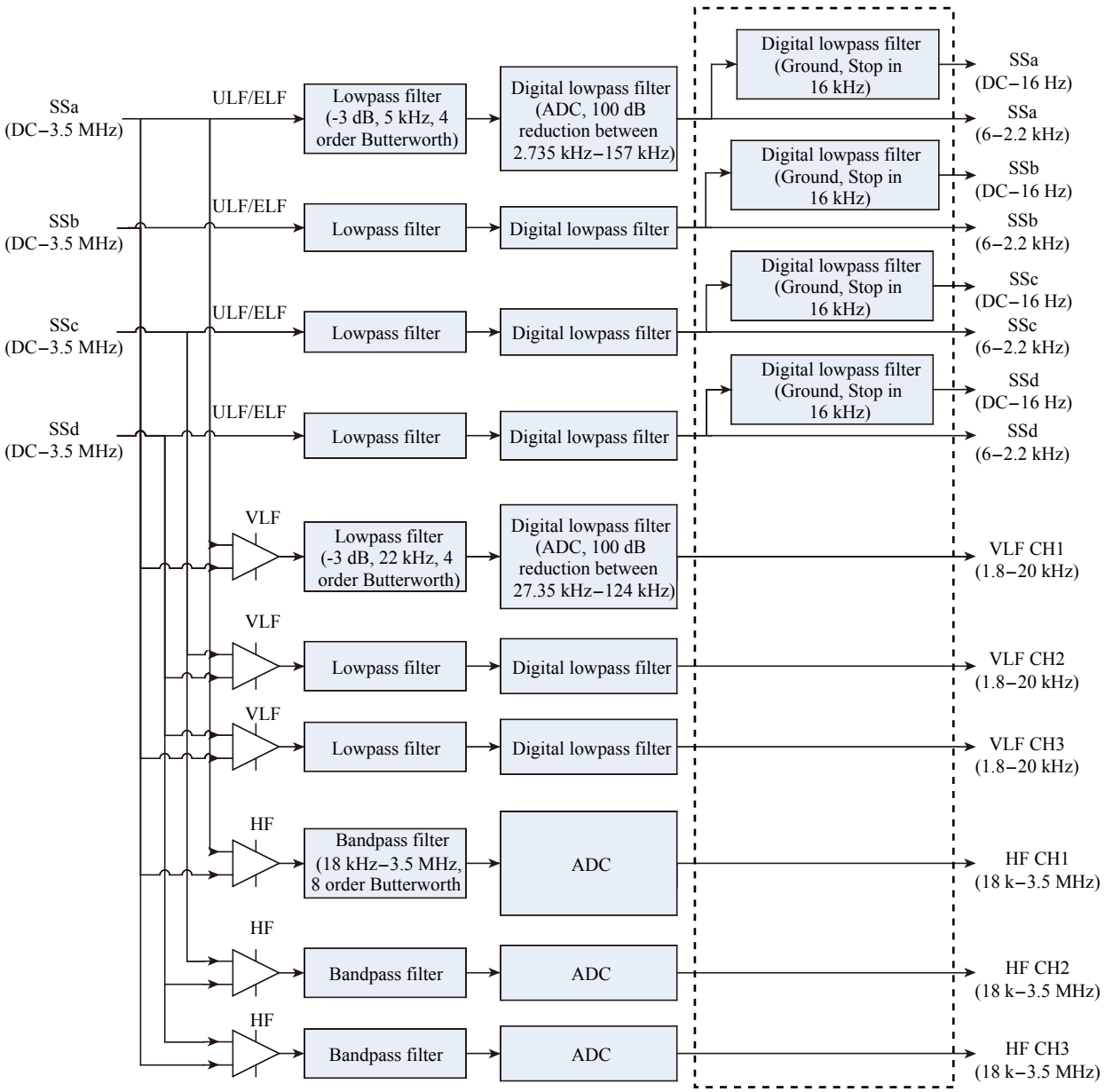

Figure 4. Detailed data acquirement progression of the EFD.

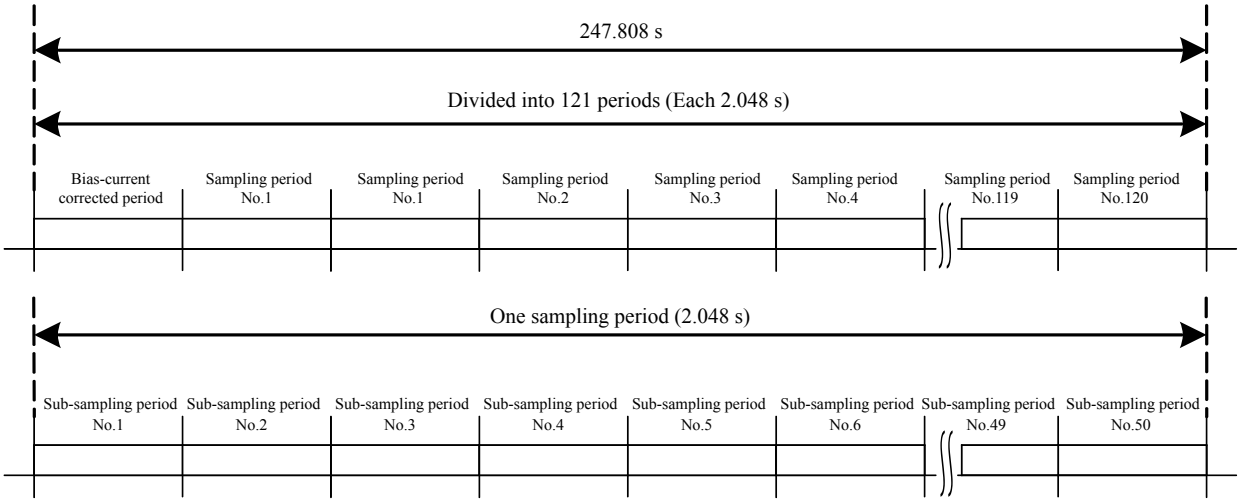

Figure 5. The onboard work time design of the EFD.

stant –400 nA.

The other 120 2.048 s sub-working periods are called sampling periods (SP), and each SP is divided equally into 50 sub-sampling periods (SSP) of 40.96 ms. The data products from DPU are different at different frequency bands.

For the ULF frequency band, the sampling rate is 125 Hz and the output data are the voltage of each probe. For the ELF frequency band, the sampling rate is 5 kHz and the outputs are each probe's voltage values. For the VLF frequency band, the sampling rate is 50 kHz, the sampling time for each SSP is 40.96 ms, which means 50 samplings in one SSP. In survey mode, the data output of the VLF band is the mean spectrum of the 50 SSPs, while in burst mode, the output is 25 waveforms of the 3-direction electric field in Payload Coordinate System (PCS). For the HF frequency band, the sampling rate is 10 MHz. In one SSP, the sampling period is only 0.2048 ms. The output data is the power spectral density. In all, the observatory data onboard satellite and the standard scientific products are listed in Table 3.

Table 3. The scientific data of EFD at different level

Band	Sampling Frequency		Level 0	Level 1	Level 2
ULF	125 Hz		4 Probe voltage	Vector electric field in SOC	Vector electric field in GEO
ELF	5 kHz		4 Probe voltage	Vector electric field in SOC	Vector electric field in GEO
VLF	50 kHz	Burst mode	Channel waveform	Vector electric field in SOC	Vector electric field in GEO
		Survey mode	Channel spectrum	Channel spectrum	Channel spectrum
HF	10 MHz		Channel spectrum	Channel spectrum	Channel spectrum

3. In-flight Performances

The test results of the EFD's in flight performances since launch of the satellite are shown in Table 4. The EFD actually measures the electric field at frequency bands from 0.5 Hz to 5 MHz. Test results from 0.5 Hz to 16 Hz show EFD resolution of 1μV·m^{-1}, satisfying the designed technical requirements. The sensitivity in flight is 0.1 μV·m^{-1}·Hz$^{-1/2}$ from 6 Hz to 2.2 kHz, 0.05 μV·m^{-1}·Hz$^{-1/2}$ from 1.8 kHz to 20 kHz, and 0.1 μV·m^{-1}·Hz$^{-1/2}$ from 18 kHz to 5 MHz. The dynamic range between DC to 20 kHz is ±1 V·m^{-1}, while at higher frequencies (20 kHz to 5 MHz) it is ±0.1 V·m^{-1}.

Table 4. In-flight performances of the EFD on ZH-1

No	Performance	Test result
1	Measurement Band	0.5 Hz–5 MHz
2	Resolution	1 μV·m^{-1} (0.5–16 Hz)
3	Sensitivity	0.1 μV·m^{-1}·Hz$^{-1/2}$ (6 Hz–2.2 kHz) 0.05 μV·m^{-1}·Hz$^{-1/2}$ (1.8 kHz–2 0 kHz) 0.1 μV·m^{-1}·Hz$^{-1/2}$ (18 kHz–5 MHz)
4	Dynamic Range	±1 V·m^{-1} (DC-20 kHz) ±0.1 V·m^{-1} (20 kHz–5 MHz)

The overall noise level over the entire frequency range (0.5 Hz to 5 MHz) is shown in Figure 6, taking the orbit 2423 (ascending) as example. Figure 6 shows that the overall noise level throughout the entire working frequency range is good, except for some regions of overlap between frequency bands.

Resolution at the ULF band is shown in Figure 7, from which it can be seen that the standard deviation of the ULF band is below 1 μV·m^{-1}, computing the data in one work period of about 2.048 s.

The SD (standard variation) based on the yellow part is 0.98 μV·m^{-1}, lower than 1 μV·m^{-1}, which is the CSES project index.

The sensitivity of the ELF/VLF/HF frequency bands, recorded by orbit No. 2423, is shown in Figure 8. Orbit No. 2423 recorded data

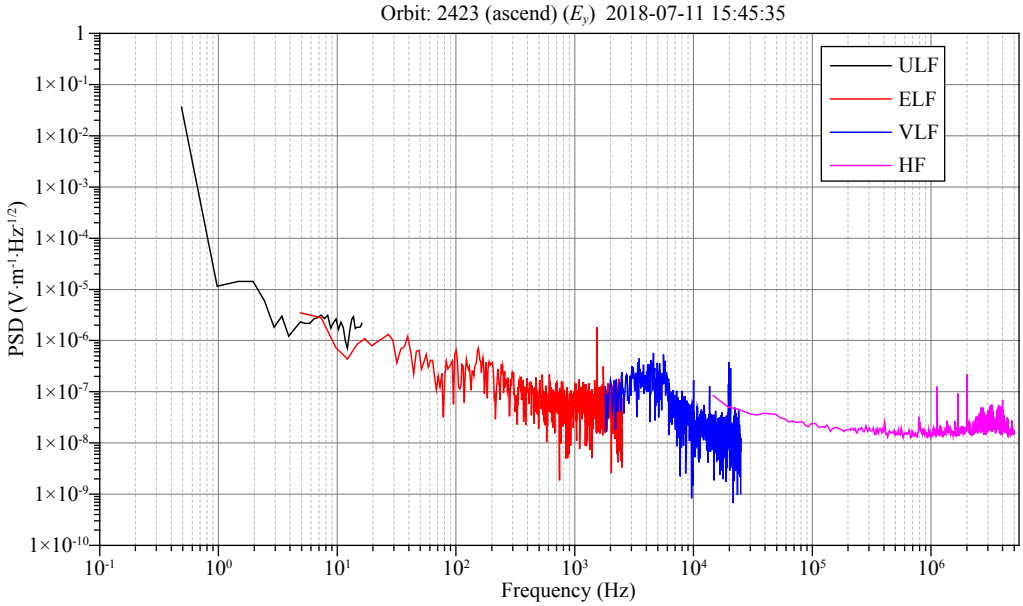

Figure 6. In-flight noise level for ULF, ELF, VLF and HF (computed by measurements during orbit No.2423 ascending).

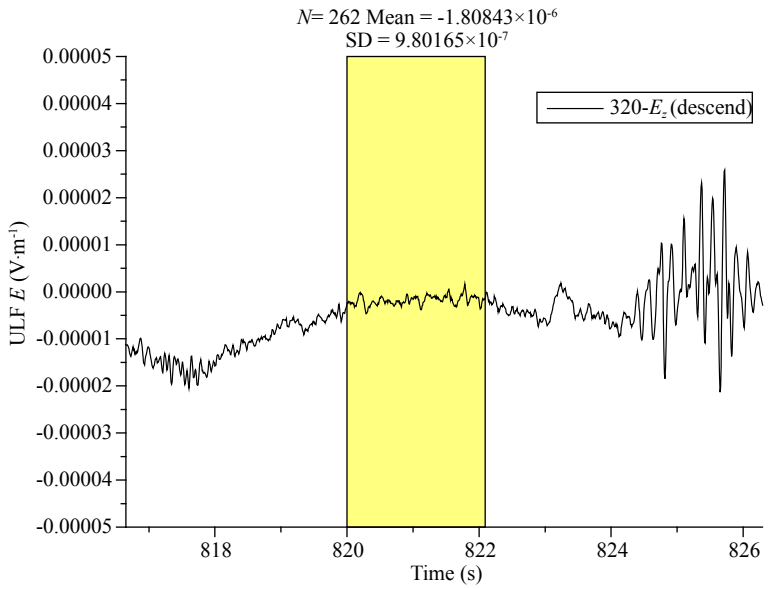

Figure 7. ULF resolution based on the electricity waveform (computed from data collected in orbit No.320 descending).

during a geomagnetic quiet time, so we can test the electric field noise lever in plasma. Specifically, at the ELF band, the noise is about 0.1 μV·m^{-1}·Hz$^{-1/2}$, and at the VLF/HF bands and HF band, the noise is about 0.05 μV·m^{-1}·Hz$^{-1/2}$.

4. First Results and Preliminary Analysis

The orbit test results obtained during the first 6 months of flight are generally good, suggesting that the EFD meets the scientific objectives of the ZH-1 satellite. Taking the orbit No. 320 (descending) as example, the raw voltage output of the four probes exhibits some natural disturbance in the electric field, meaning that the EFD can detect small wave fluctuations, as shown in Figure 9.

Figure 10 and Figure 11 show EFD measurements at the ELF and VLF bands, respectively. From the spectrum of the ELF band (Figure 10) it can be seen that there are significant enhancements close to the proton cyclotron frequency (about 600 Hz), especially at the high latitude region. Figure 11 shows strong emissions over a broad frequency band, which may be related to lightning activities, similar to DEMETER's observations of lightning activities (Zeren ZM et al., 2017).

VLF/HF radio waves emitted by ground-based transmitters provide us a good way to test the capability of in-flight instruments, for the VLF/HF radio waves propagate in the wave guide of lithosphere–ionosphere. Under certain conditions the radio waves can penetrate through the sub-ionospheric layer, propagating up to the satellite's orbit, and can be recorded by satellites (Shen XH

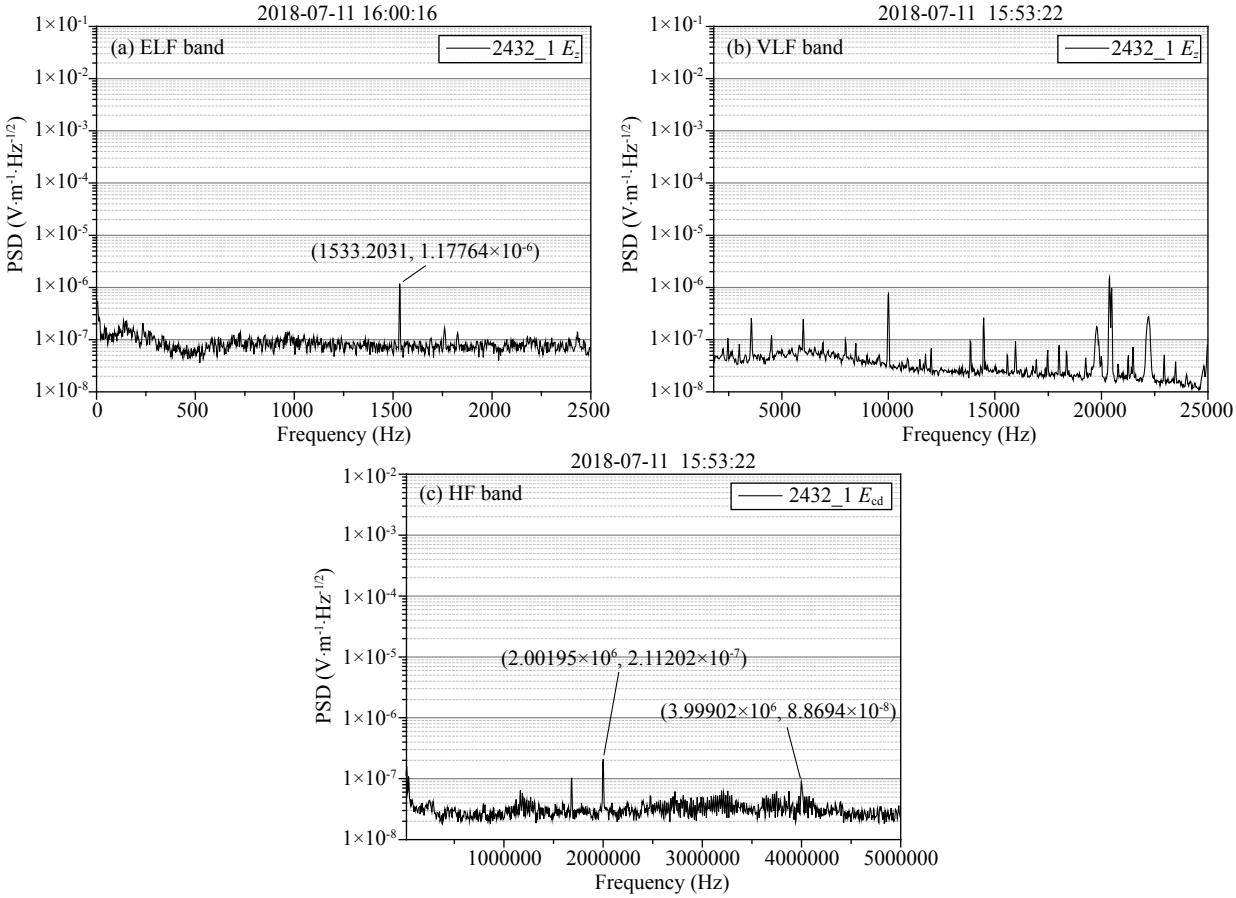

Figure 8. The sensitivity at ELF/VLF/HF bands based on the PSD (computed by orbit No.2432 ascending). (a) ELF band; (b) VLF band; (c) HF band.

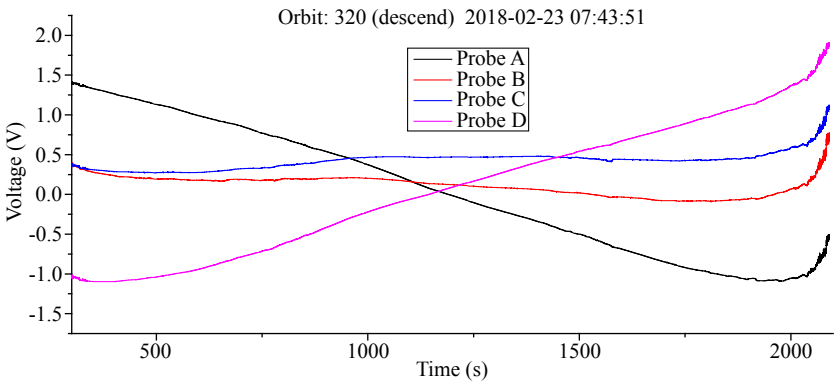

Figure 9. Small fluctuation from the EFD potential waveform from four probes (orbit No.320 descending).

et al., 2017). We chose some active ground based VLF/HF transmitters to check the EFD's capabilities. Table 5 shows the ground-based transmitters that emitted radio waves at frequency bands detected by the EFD's instruments.

Taking HWU and NWC as examples, which are shown in Figure 12, we plot the power spectrum density values at frequencies the same as the radio waves emitted by HWU (18.31 kHz), and NWC (19.8 kHz) in global map. The spectrum intensity at 18.31 kHz is significantly enhanced when the satellite flies over the HWU station. It is worth noting that the high-power NWC station also propagates radio waves to the northern conjugate position, and these signals were recorded by the EFD. The EFD can clearly detect the ground-based VLF/HF radio waves, as have other previous satellites, e.g., DEMETER.

5. Conclusion

This paper briefly presents the scientific objectives and configuration of the EFD onboard the ZH-1 satellite. In-flight test results indicate that the overall performance of the EFD is superior to other similar satellite payloads; in particular, the EFD monitors a broader frequency band, and has higher frequency resolution and sensitivity than most previous satellite missions. The EFD instrument

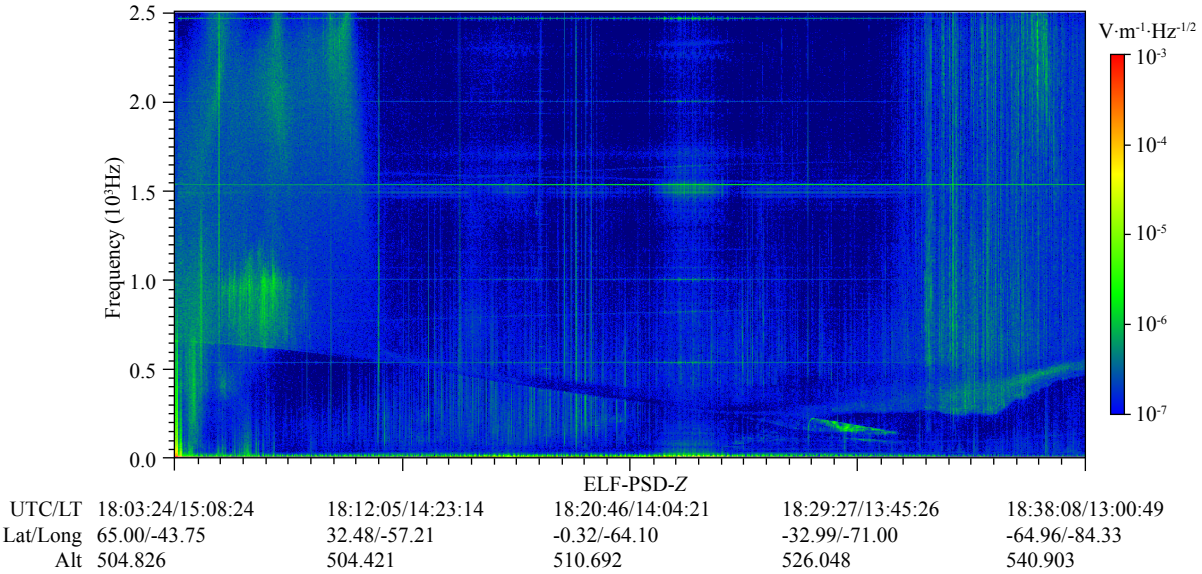

Figure 10. The time-frequency PSD at the ELF frequency band (orbit No.2425 descending).

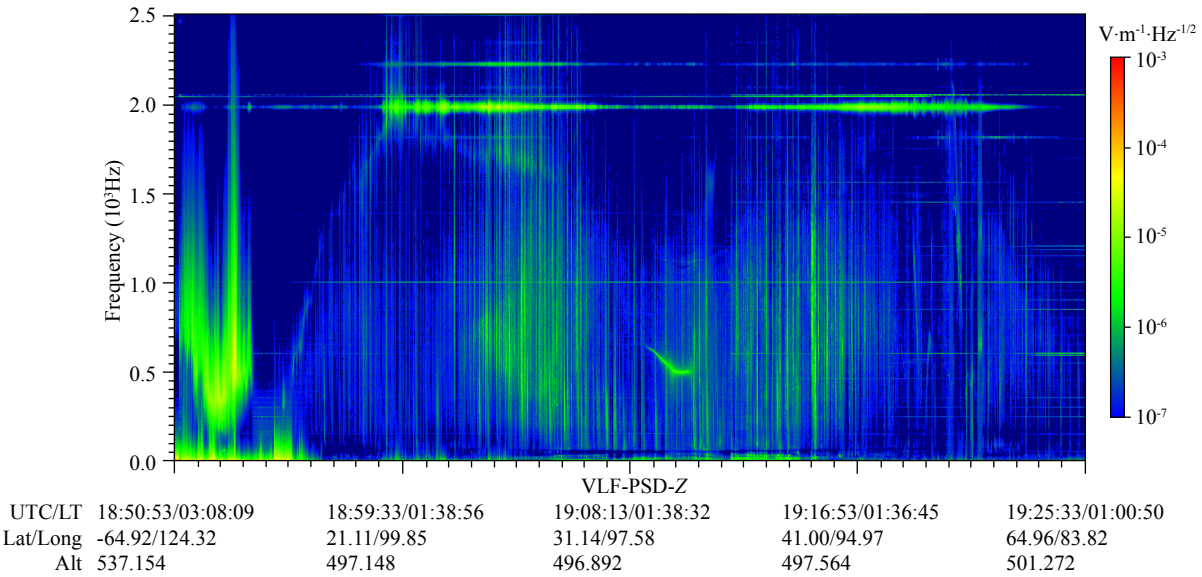

Figure 11. The time-frequency PSD at VLF band (orbit No.2425 descending).

Table 5. The transmitter's work frequency EFD detected (2018-4-23–2018-4-28)

Transmitter	Latitude (°)	Longitude (°)	Work frequency (kHz)	The frequency of EFD detected (kHz)
HWU	46.71	1.25	18.3	18.3
GBZ	54.91	–3.28	19.58	19.58
NWC	–21.82	114.17	19.8	19.8
ICV	48.92	9.73	20.27	20.27
NPM	21.42	–158.15	21.4	21.4
DHO	53.08	7.62	23.4	23.4
NAA	44.65	–67.28	24.0	24.0
NLK	48.02	–121.90	24.8	24.8

aboard the ZH-1 satisfies the requirements of the satellite's scientific objectives. Together, the ZH-1's EFD, magnetic search coil (SCM), and the high energy particle detector (HEPD), bring to the scientific community excellent opportunities to understand the

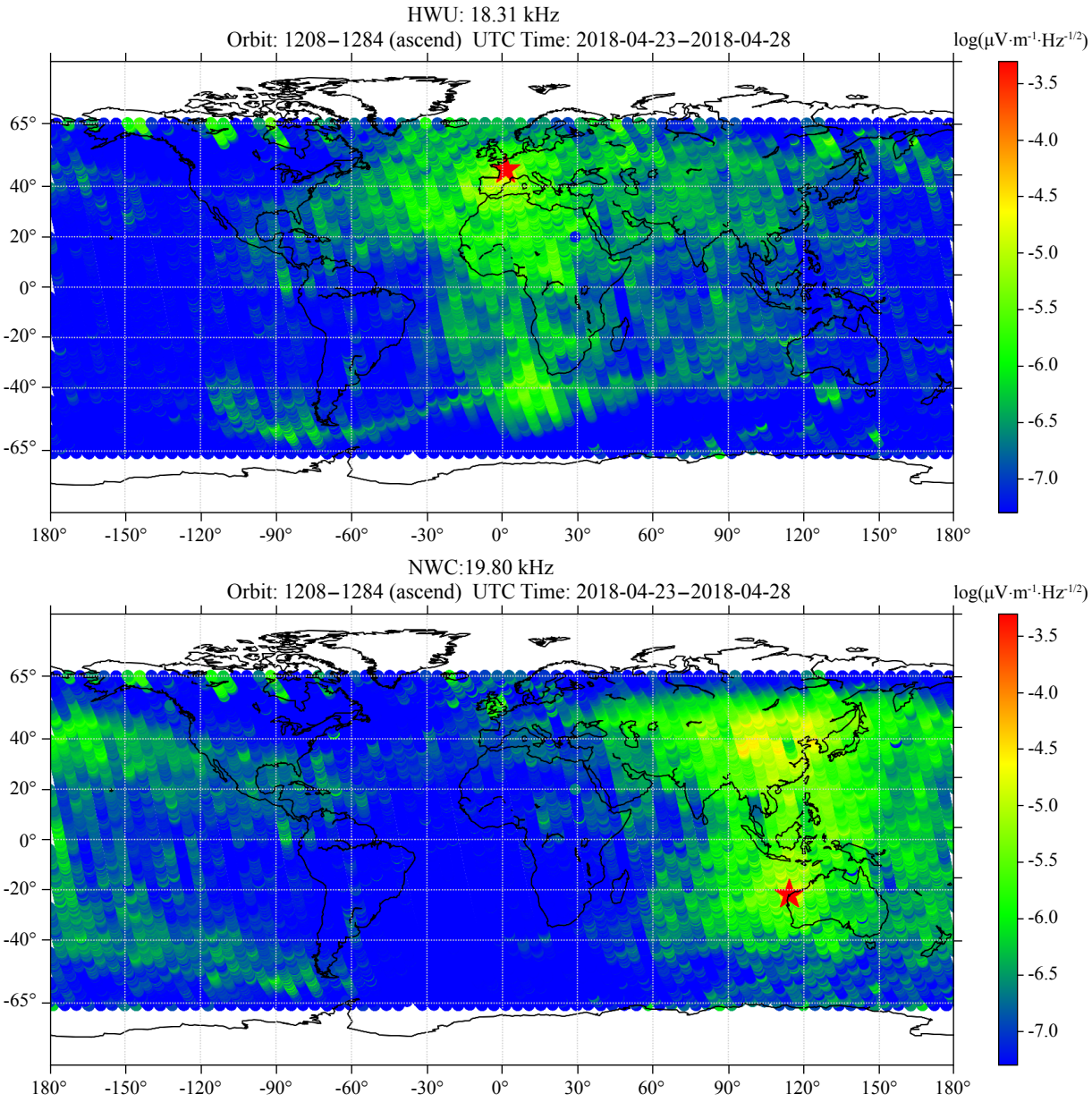

Figure 12. Electric PSD response to ground-based transmitters HWC (top) NWC (bottom). Red stars represent the locations of the transmitters.

physical mechanism of wave propagation and wave-particle coupling.

Acknowledgment

This work was supported by the civil space research project (ZH-1 data validation: Ionospheric observatory theory) and NFSC grants 41574139 and 41874174. This work made use of data from the ZH-1 mission, a project funded by the China National Space Administration (CNSA) and China Earthquake Administration (CEA).

References

Berthelier, J. J., Godefroy, M., Leblanc, F., Malingre, M., Menvielle, M., Lagoutte, D., Brochot, J. Y., Elie, C. F., Legendre, C., … Pfaff, R. (2005). ICE, the electric field experiment on DEMETER. *Planetary and Space Science*, *54*(5), 456–471. https://doi.org/10.1016/j.pss.2005.10.016

Bhattacharya, S., Sarkar, S., Gwal, A. K., Parrot, M. (2007). Observations of ULF/ELF anomalies detected by DEMETER satellite prior to earthquakes. *Indian Journal of Radio & Space Physics.*, 36(2), 103–113. http://nopr.niscair.res.in/handle/123456789/4700

Biagi, P. F., Piccolo, R., Ermini, A., Martellucci, S., Bellecci, C., Hayakawa, M., Capozzi, V., Kingsley, S. P. (2001). Possible earthquake precursors revealed by LF radio signals. *Nat. Hazards Earth Syst. Sci.*, *1*(1-2), 99–104. https://doi.org/10.5194/nhess-1-99-2001

Fraser-Smith, A.C., Bernardi, A., McGill, P. R., Ladd, M. E., Helliwell, R. A., Villard, Jr. O. G. (1990). Low-frequency magnetic field measurements near the epicenter of the Ms 7.1 Loma Prieta earthquake. *Geophys. Res. Lett.*, *17*, 1465–1468. https://doi.org/10.1029/GL017i009p01465

Hayakawa, M., Kasahara, Y., Nakamura, T., Muto, F., Horie, T., Maekawa, S., Hobara, Y., Rozhnoi, A. A., Solovieva, M., Molchanov, O. A. (2010). A statistical study on the correlation between lower ionospheric perturbations as seen by subionospheric VLF/LF propagation and earthquakes. *J. Geophys. Res.*, *115*(A9), A09305. https://doi.org/10.1029/2009JA015143

Kasahara, Y., Muto, F., Horie, T., Yoshida, M., Hayakawa, M., Ohta, K., Rozhnoi, A., Solovieva, M., Molchanov, O. A. (2008). On the statistical correlation

between the ionospheric perturbations as detected by subionospheric VLF/LF propagation anomalies and earthquakes. *Nat. Hazards Earth Syst. Sci.*, *8*(4), 653–656. https://doi.org/10.5194/nhess-8-653-2008

Maekawa, S., Horie, T., Yamauchi, T., Sawaya, T., Ishikawa, M., Hayakawa, M., Sasaki, H. (2006). A statistical study on the effect of earthquakes on the ionosphere, based on the subionospheric LF propagation data in Japan. *Ann. Geophys.*, *24*(8), 2219–2225. https://doi.org/10.5194/angeo-24-2219-2006

Molchanov, O. A., Mazhaeva, O. A., Goliavin, A. N., Hayakawa. (1993). Observation by the Intercosmos-24 satellite of ELF-VLF electromagnetic emissions associated with earthquake. *Ann. Geophs.*, *11*, 431–440.

Ouyang, X. Y., and Shen, X. H. (2015). A method for pre-processing ULF electric field disturbances observed by DEMETER and its case application analysis. *Acta Seismol. Sin.* (*in Chinese*), *37*(5), 820–829. https://doi.org/10.11939/jass.2015.05.010

Parrot, M. (1995). Use of satellites to detect seismo-electromagnetic effects. *Advances. in Space Research*, *15*(11), 271337–351347. https://doi.org/10.1016/0273-1177(95)00072-M

Rozhnoi, A., Solovieva, M., Molchanov, O., Biagi, P. -F., Hayakawa, M., Schwingenschuh, K., Boudjada, M., Parrot, M. (2010). Variations of VLF/LF signals observed on the ground and satellite during a seismic activity in Japan region in May–June 2008. *Nat. Hazards Earth Syst. Sci.*, *10*(3), 529–534. https://doi.org/10.5194/nhess-10-529-2010

Sarkar, S., and Gwal, A. K. (2010). Satellite monitoring of anomalous effects in the ionosphere related to the great Wenchuan earthquake of May 12, 2008. *Nat. Hazards*, *55*(2), 321–332. https://doi.org/10.1007/s11069-010-9530-9

Shen, X. H., Zhima, Z, Zhao, S. F., Qian, G., Ye, Q., Ruzhin, Y. (2017). VLF radio wave anomalies associated with the 2010 Ms 7.1 Yushu earthquake. *Advances. in Space Research.*, *59*(10), 2636–2644. https://doi.org/10.1016/j.asr.2017.02.040

Shen, X. H., Zhang, X. M., Yuan, S. G., Wang, L. W., Cao, J. B., Huang, J. P., Zhu, X. H., Piergiorgio, P., Dai, J. P. (2018). The state-of-the-art of the China Seismo-Electromagnetic Satellite mission. *Sci. China Technol. Sci.*, *8, 61*(5), 634–642. https://doi.org/10.1007/s11431-018-9242-0

Surkov, V. V., Molchanov, O. A., Hayakawa, M. (2003). Pre-earthquake ULF electromagnetic perturbations as a result of inductive seismomagnetic phenomena during microfracturing. *Journal of Atmospheric and Solar-Terrestrial Physics*, *65*(1), 31–46. https://doi.org/10.1016/S1364-6826(02)00117-7

Takano, T., Yamada, A., Sakai, K., Higasa, H., Shimakura, S. (2002). Enhancements of electromagnetic broadband noise in 50 MHz band which possibly associate with earthquakes. *J. Atmos. Electr.*, *22*(1), 23–324.

Yamada, A., Sakai, K., Yaji, Y., Takano, T., Shimakura, S. (2002). Observations of natural noise in VHF band which relates to earthquakes. In: Hayakawa, M., and Molchanov, O. A. (Eds.), *Seismo Electromagnetics* (*Lithosphere-Atmosphere-Ionosphere Coupling*) (pp. 255–257). Tokyo: Terra Scientific Publishing Company, Tokyo, 255–257.

Zeren Z. M., Cao, J. B., Liu, W. L., Fu, H. S., Wang, T. Y., Zhang, X. M., Shen, X. H. (2014). Storm time evolution of ELF/VLF waves observed by DEMETER satellite. *J. Geophys. Res.*: *Space Physics*, *119*(4), 2612–2622. https://doi.org/10.1002/2013JA019237

Zeren Z. M., Chen, L. J., Xiong, Y., Cao, J. B., Fu, H. S. (2017). On the origin of ionospheric hiss: a conjugate observation. *J. Geophys. Res.*: *Space Physics*, *122*(11), 784–793. https://doi.org/10.1002/2017JA024803

Zeren Z. M., Shen, X. H., Cao, J. B., Zhang, X. M., Huang, J. P., Liu, J., Ouyang, X. Y., Zhao, S. F. (2012). Statistical analysis of ELF/VLF magnetic field disturbances before major earthquakes. *Chinese J. Geophys.* (*in Chinese*), *55*(11), 3699–3708.

Zhang, X., Shen, X. M., Parrot, M., Zeren, Z., Ouyang, X., Liu, J., Qian, J., Zhao, S., Miao, Y. (2012). Phenomena of electrostatic perturbations before strong earthquake (2005-2010) observed on DEMETER. *Nat. Hazards Earth Syst Sci.*, *12*(1), 75–83. https://doi.org/10.5194/nhess-12-75-2012

Zhang, X., Shen, X. H., Zhao, S. F., Lu, Yao., Ouyang, X. Y., Qian, J. D. (2014). The characteristics of quasistatic electric field perturbations observed by DEMETER satellite before large earthquakes. *Journal of Asian Earth Sciences*, *79*(A), 42–52. https://doi.org/10.1016/j.jseaes.2013.08.026

Zhang, X., Zeren, Z., Parrot, M., Battiston, R., Qian, J., Shen, X. (2011). ULF/ELF ionospheric electric field and plasma perturbations related to Chile earthquakes. *Advances in Space Research*, *47*(6), 991–1000. https://doi.org/10.1016/j.asr.2010.11.001